Critical Current Densities through Josephson Junctions in Low Magnetic Fields

Bradley P. Din, Alexander I. Blair, Frank Schoofs, Damian P. Hampshire

***Abstract*—Understanding the properties of grain boundaries in polycrystalline superconductors is essential for optimizing their critical current density. Here, we provide computational simulations of 2D Josephson junctions (JJs) in low magnetic fields using time–dependent Ginzburg–Landau theory, since they can be considered a proxy for a grain boundary between two grains. We present data for junctions with a wide range of superconducting electrodes of different Ginzburg–Landau parameter (κ) values and geometries, as well as normal barriers with different strengths of pair–breaking — characterized by the thickness of the junction and the junction condensation parameter ($\tilde{\alpha}_\mathrm{n}$). We describe our results using analytic solutions, and hence provide a detailed description of Josephson junctions in low fields up to that required for a single fluxon to penetrate the junction.**

***Index Terms*—Josephson Junctions, Critical Currents**

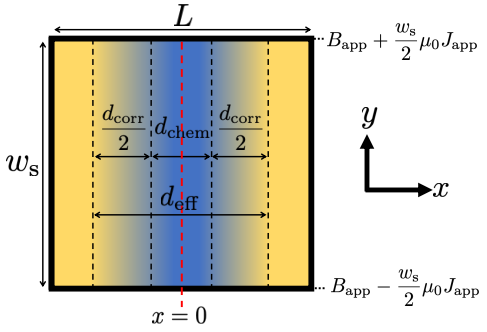

Fig. 1: A SNS Josephson junction with a system aspect ratio, L/w_s, of unity. The superconducting electrode is shown in yellow and the normal junction in blue.

I. Introduction

LOW temperature polycrystalline superconductors are the enabling technology for many commercial applications, such as fusion tokamaks [1] operating above 10 T. However, there is still a huge scope for improving their performance — for example, the critical current density (J_c) of $\mathrm{Nb_3Sn}$ is less than 1% of the depairing current in high magnetic fields [2]. Understanding the grain boundaries that provide the flux pinning [3] is pivotal for high-field applications. In this paper we investigate the properties of superconductor–normal–superconductor (SNS) 2D Josephson junctions (JJs) [4], [5] because of their utility as a model for grain boundaries in a polycrystalline superconductor [6]. We use time–dependent Ginzburg–Landau (TDGL) simulations to produce the field dependence of J_c and summarize our results using analytic solutions. We discuss the insights and limitations of these solutions. Finally, we outline our future work.

II. Critical Current Solutions

The starting point for all the simulations presented in this work are the normalized TDGL equations [7]–[10]. In the zero electric potential gauge, they are written in the form

$$\eta\frac{\partial\tilde{\psi}}{\partial\tilde{t}} = \left[\frac{1}{\tilde{m}_\mathrm{n}}(\tilde{\boldsymbol{\nabla}} - \imath\tilde{\boldsymbol{A}})^2 + \tilde{\alpha}_\mathrm{n} - \tilde{\beta}_\mathrm{n}\left|\tilde{\psi}\right|^2\right]\tilde{\psi}, \tag{1}$$

$$\frac{\partial\tilde{\boldsymbol{A}}}{\partial\tilde{t}} = -\kappa^2\tilde{\boldsymbol{\nabla}}\times\tilde{\boldsymbol{\nabla}}\times\tilde{\boldsymbol{A}} + \mathrm{Im}\left[\tilde{\psi}^*(\tilde{\boldsymbol{\nabla}} - \imath\tilde{\boldsymbol{A}})\tilde{\psi}\right], \tag{2}$$

with the corresponding boundary conditions [11]:

$$\left(\tilde{\boldsymbol{\nabla}}\times\tilde{\boldsymbol{A}} - \tilde{\boldsymbol{B}}_{\mathrm{app}}\right)\times\hat{\boldsymbol{n}} = 0, \tag{3}$$

$$\left(\tilde{\boldsymbol{\nabla}} - \imath\tilde{\boldsymbol{A}}\right)\tilde{\psi}\cdot\hat{\boldsymbol{n}} = \frac{1}{\tilde{b}}\tilde{\psi}. \tag{4}$$

Spatial dimensions are normalized by the coherence length, $\xi_\mathrm{s} = \hbar/\sqrt{-2m_\mathrm{s}\alpha_\mathrm{s}}$, time by $\tau = \mu_0\kappa^2\xi_\mathrm{s}^2/m_\mathrm{s}$ and supercurrent densities by $J_0 = B_{\mathrm{c2}}/\mu_0\xi_\mathrm{s}\kappa^2$ [12], [13]. The depairing current density, J_D, is given by $J_\mathrm{D} = \left(2/3\sqrt{3}\right)J_0$ [14]. Electric fields are normalized by E_D (the electric field at J_D), the order parameter by the bulk Meissner value, $\psi_0 = \sqrt{-\alpha_s/\beta_s}$, and the magnetic field by the upper critical field, $B_{\mathrm{c2}} = \phi_0/2\pi\xi_s^2$, where ϕ_0 is the flux quantum, $\phi_0 = h/2e$ [15]. All other symbols have their usual definitions [14], [16]. The variation of $\tilde{m}_\mathrm{n}$, $\tilde{\alpha}_\mathrm{n}$ and $\tilde{\beta}_\mathrm{n}$ allows for the spatial variation in the critical temperature, T_c, within the system, enabling the modeling of inhomogenous systems such as SNS junctions where the normal barrier has a lower T_c than the superconducting electrodes [17]. For all simulations here, we have taken $\tilde{m}_\mathrm{n} = 1$, $\tilde{\beta}_\mathrm{n} = 1$ and the standard dirty limit value for $\eta = 5.79$ [7], [18].

For a 2-dimensional SNS junction as shown in Fig. 1, Clem has provided solutions for $J_\mathrm{c}(B)$ for superconducting electrodes with different aspect ratios using the Josephson relation [5],

$$\frac{J_\mathrm{c}(\tilde{B})}{J_\mathrm{c}(0)} = \frac{1}{\tilde{w}_s}\left|\int_{-\tilde{w}_s/2}^{\tilde{w}_s/2}\sin(\Delta\gamma(\tilde{y}))\,\mathrm{d}\tilde{y}\right|. \tag{5}$$

Manuscript receipt and acceptance dates will be inserted here. This work is funded by EPSRC grant EP/L01663X/1 that supports the EPSRC Centre for Doctoral Training in the Science and Technology of Fusion Energy.

BPD and DPH are with the Durham University Superconductivity Group, Centre for Material Physics, Department of Physics, Durham University, UK.

AIB and FS are with the United Kingdom Atomic Energy Authority, Culham Science Centre, Abingdon, UK.

Color versions of one or more of the figures in this paper are available online at http://ieeexplore.ieee.org.

Digital Object Identifier will be inserted here upon acceptance.

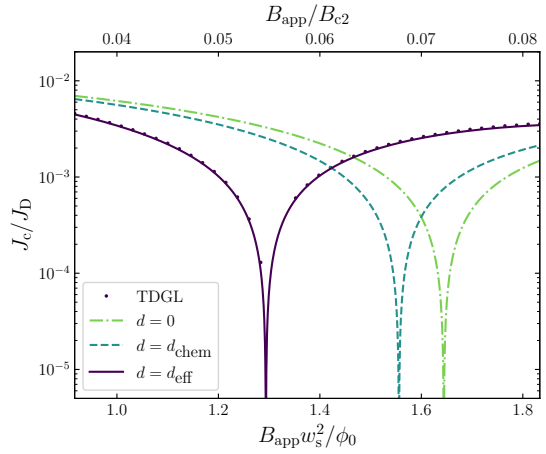

Fig. 2: Critical current density as a function of applied magnetic field, compared to Eq. (6), for $d = 0\xi_s$, $d = d_{chem} = 0.5\xi_s$ and $d = d_{eff} = 2.55\xi_s$. TDGL parameters are $L = w_s = 12.0\xi_s$, $\tilde{\alpha}_n = -50.0$, $\kappa = 36$, $\delta t = 0.1\tau$ and $h_x = h_y = 0.1\xi_s$.

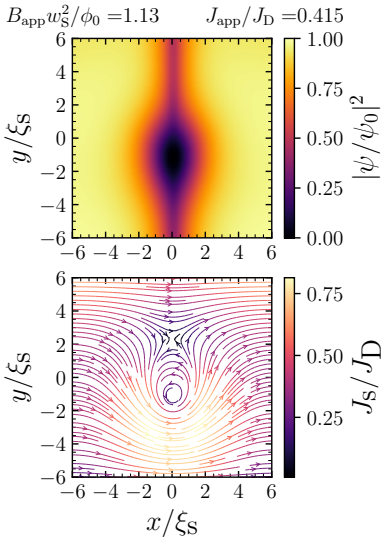

Fig. 3: A snapshot of normalized order parameter magnitude (top) and supercurrent density (bottom) in a SNS junction at $J_{app} = J_c$. TDGL parameters are $L = w_s = 12.0\xi_s$, $d_{chem} = 0.5\xi_s$, $\tilde{\alpha}_n = -1.0$, $\kappa = 40.0$, $\delta t = 0.5\tau$ and $h_x = h_y = 0.1\xi_s$.

Here, $J_c(0)$ is the critical current density in zero field, $\Delta\gamma$ is the gauge invariant phase difference across the junction and the maximum Josephson current occurs when the constant $\Delta\gamma(y = 0) = \pm\pi/2$. Clem assumed that the order parameter recovers instantaneously within the electrode to the bulk Meissner value, implicitly assuming that the coherence length of the superconductor was much smaller than any system dimensions. Recent work in our group [19] has extended Clem's work to consider finite coherence length and found the result for the gauge invariant phase difference for a junction of finite thickness to be

$$\Delta\gamma(\tilde{y}) = \Delta\gamma(0) + \tilde{B}_{app}\tilde{y}\tilde{d} + \frac{8\tilde{B}_{app}}{\tilde{w}_s}\sum_{n=0}^{\infty}\frac{(-1)^{n+1}}{k_n^3}\tanh\left(k_n\frac{\tilde{L}-\tilde{d}}{2}\right)\sin\left(k_n\tilde{y}\right), \quad (6)$$

where $k_n = 2\pi(n + 1/2)/\tilde{w}_s$ and the term $\tilde{d}$ in Eq. (6) was replaced by $\tilde{d}_{eff}$ to account for the region in each electrode, of approximately one coherence length, over which the order parameter increases up to its bulk value. The effective junction thickness $\tilde{d}_{eff}$ is defined using

$$\tilde{d}_{eff} = \tilde{d}_{chem} + \tilde{d}_{corr}, \quad (7)$$

where $\tilde{d}_{chem}$ is the chemical thickness of the barrier that describes the region with the normal state Ginzburg–Landau parameters ($\tilde{\alpha}_n$ and $\tilde{\beta}_n$), and $\tilde{d}_{corr}$ is the correction term that accounts for the additional thickness of the barrier. We note that the effective electrode length is $\tilde{L} - \tilde{d}_{eff}$.

In Fig. 2, we provide a comparison between Eq. (6) with different values of $\tilde{d}$ and TDGL simulations for low J_c junctions ($\tilde{\alpha}_n = -50.0$) with a chemical thickness of $d_{chem} \approx 0.5\xi_s$. These results are consistent with previous results [19] that found $d_{corr} \approx 2\xi_s$ provides the best fit.

III. Computational Methodology

The computational algorithm used in these simulations solves the TDGL equations in the zero electric potential gauge [7], [17], [20] and has been discussed extensively in previous publications [9], [13], [19]. In brief, the TDGL equations are solved using a finite–difference method based on the method of link variables [21], which ensures gauge invariance of the system. The 2-dimensional system is discretized into a set of regular nodes on a grid in units of the coherence length, determined by the grid spacing in each of the x and y directions, $\tilde{h}_x$ and $\tilde{h}_y$ respectively. The variables $\{\tilde{\psi}, \tilde{\boldsymbol{A}}\}$ are continually iterated until convergence to within a specified tolerance (set to 10^{-7} within this work). For evolving this set of variables forward in time, we use a modified Crank–Nicolson scheme [22], using a fixed time step, δt in units of τ. We have used periodic boundary conditions at the boundaries of the system in the x-direction, and insulating boundary conditions in the y-direction using a ghost point method [23].

To obtain a value for J_c, we increase the transport current at a specified ramp rate and monitor the average electric field in the x direction within the system, $\langle\tilde{E}_x\rangle$ [8]. We apply Ekin's offset criterion method [24]; if $\langle\tilde{E}_x\rangle$ exceeds a fixed critical electric field $\tilde{E}_c$, then the system is held at this applied current value for a fixed duration to allow transient effects to equilibriate. If the electric field persists beyond the duration of the hold time, then we interpret this as persistent fluxon motion — the tangent to the $\tilde{E}(\tilde{J})$ is extrapolated to zero electric field and the critical current density, $\tilde{J}_c$, is taken at this point. The system is first initialized in the Meissner state ($\tilde{\psi} = 1$, $\tilde{B} = 0$) for reproducibility of simulations. In this work, the electric field criterion is set at $\tilde{E}_c = 10^{-6}$ and the hold time is set at $6 \times 10^4\tau$.

The outputs from our methodology include the spatial dependence of the order parameter and the magnetic vector potential. These provide visualizations of useful physical phenomena, such as fluxon motion within the junction and the associated changes in the supercurrents. A snapshot of these

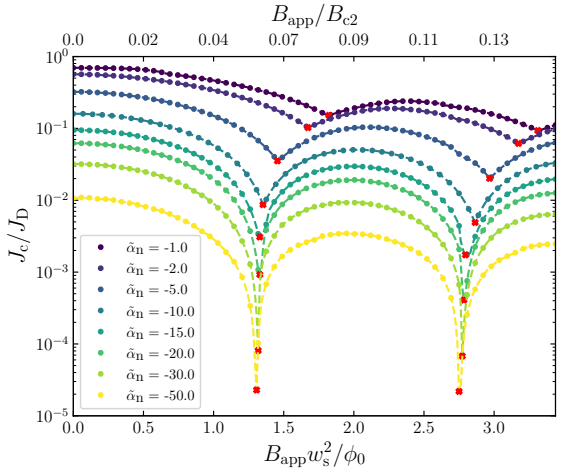

Fig. 4: Critical current density as a function of applied magnetic field for a range of $\tilde{\alpha}_n$ values in a SNS junction system. TDGL parameters are $\kappa = 36$, $L = w_s = 12.0\xi_s$, $d_{chem} = 0.5\xi_s$. Red crosses denote the minima of J_c.

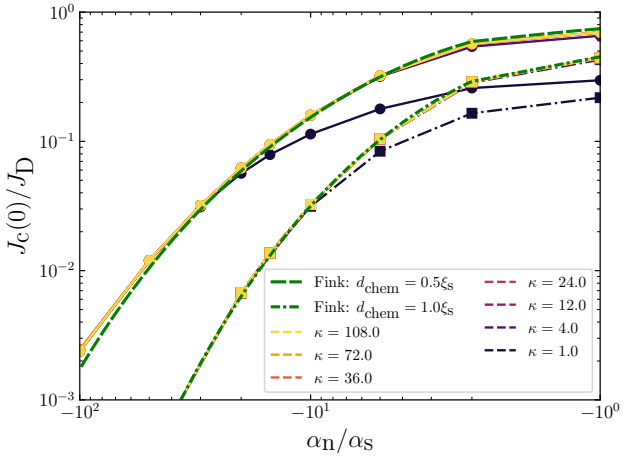

Fig. 5: Zero–field critical current density as a function of $\tilde{\alpha}_n$, for a range of κ values, for two SNS junctions: $d_{chem} = 0.5\xi_s$ are circles (solid lines) and $d_{chem} = 1.0\xi_s$ are squares (dashed–dotted lines). Both geometries have $L = w_s = 12.0\xi_s$. Green lines are Fink's very narrow solutions [27] for each d_{chem}.

outputs for a typical SNS system is shown in Fig. 3. We can see as expected: despite the transport critical current density being only $0.4J_D$, the magnitude of the local supercurrent densities can be as large as $0.8J_D$; the presence of a fluxon within the junction causes large additional local current flows; the fluxon itself is distorted within the junction, extending into a region much wider than the chemical thickness, with similarities to the 'pancake' vortices first discussed by Clem [25].

IV. Results

Here we are particularly interested in the first node, or minima, in J_c because it allows a precise characterization of the effective thickness of the normal barrier. We have completed $J_c(B)$ simulations for JJs with a wide range of electrodes of different κ values and for different strengths of the pair–breaking in the normal barriers (i.e. two different thicknesses and different junction condensation parameter values, $\tilde{\alpha}_n$). De Gennes has shown that increasing $|\tilde{\alpha}_n|$ decreases the coherence length in the normal region [11]. Here we have set $h_x = h_y = 0.1\xi_s$ since too large of a grid size can lead to error [26]. Junctions with very weak coupling (i.e. high $|\tilde{\alpha}_n|$) also require small timesteps for accurate convergence. We have used $\delta t = 0.02\tau$ for data with $\tilde{\alpha}_n = -50.0$ or -100.0, and $\delta t = 0.1\tau$ for all other values of $\tilde{\alpha}_n$.

In Fig 4, we show the results for a system where $L = w_s = 12.0\xi_s$ and the chemical junction thickness is set to be $d_{chem} = 0.5\xi_s$. The red crosses are located at minima of J_c; we denote the field for the first minimum to be B_{min}. As $\tilde{\alpha}_n \to -\infty$, B_{min} decreases to an asymptotic value at high κ, consistent with flux entering the junction more easily, increased pair–breaking within the junction and the reduction in the zero–field critical current density, $J_c(0)$.

In Fig. 5, we compare the zero–field critical current density of our TDGL simulations to analytic solutions from Fink [27] that were derived in the very narrow regime ($w_s \ll \xi_s$) for thick, weakly–coupled junctions. Agreement between these analytic

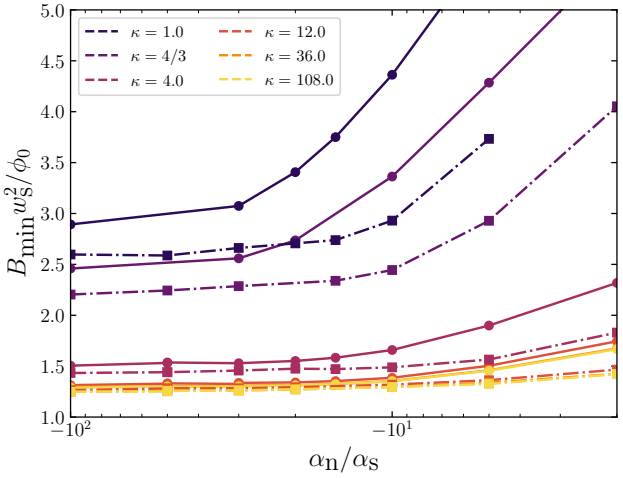

Fig. 6: B_{min} as a function of $\tilde{\alpha}_n$, for a range of κ values. The symbols associated with each geometry are the same as Fig. 5.

solutions and TDGL computation has previously been verified for very narrow junctions, and found to extend to narrow junctions [19]. Here we compare Fink's analytic solutions to data for narrow junctions with variable κ and two chemical junction thicknesses. Fink's solutions remain valid for high κ and very large $|\tilde{\alpha}_n|$, but at low κ, when the junction width approaches the wide junction limit ($w_s \gg \xi_s, \lambda_s$, where λ_s is the penetration depth), the agreement does not hold. We attribute this low κ result to the current density flow along the SNS junction no longer being uniform across its width.

Fig. 6 shows B_{min} as a function of $\tilde{\alpha}_n$. We have computationally verified that for the $d_{chem} = 0.5\xi_s$, $L = w_s = 12.0\xi_s$ geometry, the asymptotic value of B_{min} for $\kappa = 36$ and $\tilde{\alpha}_n = -100.0$ differs from that of $\tilde{\alpha}_n = -250.0$ or $\tilde{\alpha}_n = -500.0$ by less than 1%. The values of B_{min} (and consequently d_{eff}) change with κ.

We can find an analytic expression for B_{min} in terms of d_{eff}

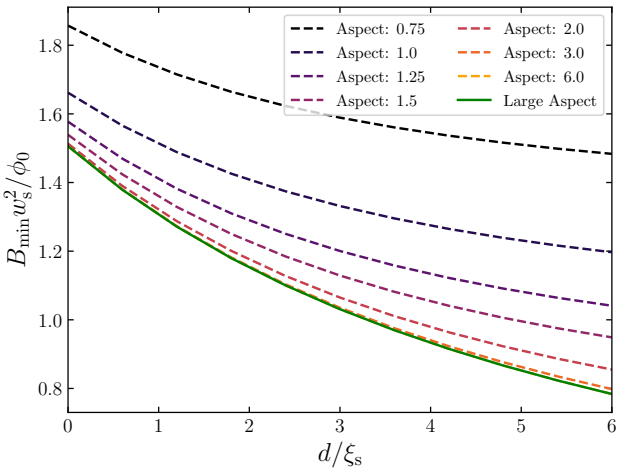

Fig. 7: $B_{\min}$ as a function of d/ξ_s, for a range of system aspect ratios (L/w_s), obtained from Eq. (11). The large aspect ratio limit solution is given by Eq. (10).

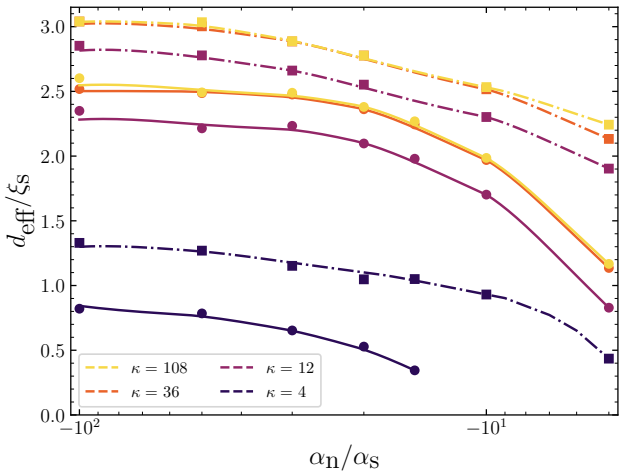

Fig. 8: d_{eff}/ξ_s as a function of $\tilde{\alpha}_n$, obtained from TDGL and using Eq. (6). The symbols associated with each geometry are the same as Fig. 5.

using Eqs. (5) and (6) where

$$B_{\min} = \frac{\phi_0 \pi}{\pi d_{\text{eff}} w_s + \frac{16\pi}{w_s} \sum_{n=0}^{\infty} \frac{\tanh[k_n(L-d_{\text{eff}})/2]}{k_n^3}}. \quad (8)$$

In the extreme cases where the aspect ratio is very small ($L/w_s \ll 1$) or very large ($L/w_s \to \infty$), we can obtain the relevant asymptotic values. For the very small (large) aspect ratio, we define $B^{\mathcal{S}}_{\min}$ ($B^{\mathcal{L}}_{\min}$) as

$$B^{\mathcal{S}}_{\min} = \frac{\phi_0}{w_s L}, \quad (9)$$

$$B^{\mathcal{L}}_{\min} = \frac{0.8173\phi_0\pi^3}{\pi^3 d_{\text{eff}} w_s + 14 w_s^2 \zeta(3)}, \quad (10)$$

respectively. We note that for the large aspect ratio limit, we have added the factor of 0.8173, taken from Clem's work [5], to account more precisely for the magnetic field at the first minima of the critical current density. Following Clem, we use his interpolating function for $B_{\min}$, between high and low aspect ratios, of the form

$$B_{\min} = \frac{B^{\mathcal{L}}_{\min}}{\tanh\left(B^{\mathcal{L}}_{\min}/B^{\mathcal{S}}_{\min}\right)}, \quad (11)$$

and have plotted it in Fig. 7. We have separately verified that the small aspect ratio limit (Eq. (9)) is obtained within 1% for $L/w_s < 0.1$.

Using the $B_{\min}$ values from our TDGL simulations, we calculated the corresponding d_{eff} values as a function of $\tilde{\alpha}_n$ using Eq. (6) as shown in Fig. 8. Hence, we conclude from the results here, that for large κ, large negative $\tilde{\alpha}_n$ and aspect ratio for the superconducting electrode of about unity, Eq. (7) can be written

$$d_{\text{eff}} \approx d_{\text{chem}} + (2.0 \pm 0.1)\xi_s, \quad (12)$$

consistent with previous results [19] and confirmed by the thicker junction data in the high κ limit, where $d_{\text{chem}} = 1.0\xi_s$, $L = w_s = 12.0\xi_s$. Fig. 8 also demonstrates that d_{eff} reduces significantly when either κ or $|\tilde{\alpha}_n|$ is small.

V. Discussion and Conclusions

In this work, we performed TDGL simulations for 2D Josephson junctions and found Fink's zero–field analytic solutions derived for very narrow junctions successfully describes our TDGL data across the entire $\tilde{\alpha}_n$ range at high values of κ for junctions with aspect ratios around unity, but breaks down at low values of κ. We have confirmed the relationship between the chemical junction thickness and the effective junction thickness in the high κ, high $|\tilde{\alpha}_n|$ limit (Eq. (12)) found previously and extended its validity to include a thicker junction barrier. Our results suggest the validity cannot be extended to wide junctions. We have also extended Clem's interpolation function to include d_{eff}.

Future work will include developing our analytic expressions further for a wider range of depairing strength in the junction (i.e. $\tilde{\alpha}_n$ and d_{chem}), and extending these solutions to finite κ. We will investigate larger systems (e.g. $L = w_s = 24.0\xi_s$ or $72.0\xi_s$) to better understand the wide junction limit and the κ-dependence of the data shown in this work. We also intend to extend this work to high fields so we can make direct comparisons with high–field experimental data. To understand high–field behavior properly, we need to consider the presence of many fluxons both inside the junction (grain boundaries) and also inside the bulk electrodes (grains).

Acknowledgment

This work was supported by the Engineering and Physical Sciences Research Council [EP/L01663X/1]. This work made use of the facilities of the Hamilton7 and Hamilton8 HPC Services of Durham University. The code is available on request from DPH. This work has been carried out within the framework of the EUROfusion Consortium and has received funding from the Euratom research and training programme 2014-2018 and 2019-2020 under grant agreement No 633053. The views and opinions expressed herein do not necessarily reflect those of the European Commission.

REFERENCES

[1] P. Bruzzone, "Superconductivity and fusion energy—the inseparable companions," *Superconductor Science and Technology*, vol. 28, no. 2, p. 024001, Dec. 2014.

[2] G. Wang, M. J. Raine, and D. P. Hampshire, "How Resistive Must Grain-Boundaries be to Limit J_c in Polycrystalline Superconductors?" *Supercond. Sci. Technol.*, vol. 30, no. 10, Aug. 2017, Art. no. 104001.

[3] W. Schauer and W. Schelb, "Improvement of Nb_3Sn High Field Critical Current by a Two-stage Reaction," *IEEE Transactions on Magnetics*, vol. 17, pp. 374–377, 1981.

[4] B. Josephson, "Possible new effects in superconductive tunnelling," *Physics Letters*, vol. 1, no. 7, p. 251–253, 1962.

[5] J. R. Clem, "Josephson junctions in thin and narrow rectangular superconducting strips," *Phys. Rev. B*, vol. 81, no. 14, Apr. 2010, Art. no. 144515.

[6] G. J. Carty and D. P. Hampshire, "Visualising the mechanism that determines the critical current density in polycrystalline superconductors using time-dependent Ginzburg-Landau theory," *Physical Review B*, vol. 77, p. 172501, 2008.

[7] A. Schmid, "A Time dependent Ginzburg-Landau Equation and its Application to the problem of resistivity in the Mixed State," *Physik der Kondensierte Materie*, vol. 5, no. 4, pp. 302–317, 1966.

[8] M. Machida and H. Kaburaki, "Direct simulation of the time-dependent Ginzburg-Landau equation for type-II superconducting thin film: Vortex dynamics and V-I characteristics," *Physical Review Letters*, vol. 71, no. 19, p. 3206–3209, 1993.

[9] A. I. Blair and D. P. Hampshire, "Time-Dependent Ginzburg–Landau Simulations of the Critical Current in Superconducting Films and Junctions in Magnetic Fields," *IEEE Transactions on Applied Superconductivity*, vol. 28, no. 4, p. 1–5, 2018.

[10] I. Sadovskyy, A. Koshelev, C. Phillips, D. Karpeyev, and A. Glatz, "Stable large-scale solver for Ginzburg–Landau equations for superconductors," *Journal of Computational Physics*, vol. 294, p. 639–654, 2015.

[11] P. G. De Gennes, *Superconductivity of Metals and Alloys*. Boulder, Colorado: Perseus Books Group, 1999.

[12] Fleckinger-Pelle, Jacqueline and Kaper, Hans G, "Gauges for the Ginzburg-Landau equations of superconductivity," Argonne National Lab., IL (United States), Tech. Rep., 1995.

[13] A. I. Blair and D. P. Hampshire, "Modeling the Critical Current of Polycrystalline Superconducting Films in High Magnetic Fields," *IEEE Transactions on Applied Superconductivity*, vol. 29, no. 5, p. 1–5, 2019.

[14] M. Tinkham, *Introduction to superconductivity*. Courier Corporation, 2004.

[15] M. Cyrot, "Ginzburg-Landau theory for superconductors," *Reports on Progress in Physics*, vol. 36, no. 2, pp. 103–158, Feb. 1973.

[16] D. R. Tilley and J. Tilley, *Superfluidity and Superconductivity*, 3rd ed. Bristol, UK: IOP, 1990, ch. 8, sec. 4, pp. 303–312.

[17] G. J. Carty, M. Machida, and D. P. Hampshire, "Numerical studies on the effect of normal metal coatings on the magnetisation characteristics of type-II superconductors," *Physical Review B*, vol. 71, p. 144507, 2005.

[18] N. Kopnin, *Theory of nonequilibrium superconductivity*. Oxford University Press, 2001, vol. 110.

[19] A. I. Blair and D. P. Hampshire, "The critical current density of SNS Josephson junctions and polycrystalline superconductors in high magnetic fields," 2021, arXiv:2110.02053.

[20] T. Winiecki and C. Adams, "A Fast Semi-Implicit Finite-Difference Method for the TDGL Equations," *Journal of Computational Physics*, vol. 179, no. 1, p. 127–139, 2002.

[21] W. D. Gropp, H. G. Kaper, G. K. Leaf, D. M. Levine, M. Palumbo, and V. M. Vinokur, "Numerical Simulation of Vortex Dynamics in Type-II Superconductors," *Journal of Computational Physics*, vol. 123, no. 2, p. 254–266, 1996.

[22] J. Crank and P. Nicolson, "A practical method for numerical evaluation of solutions of partial differential equations of the heat-conduction type," *Mathematical Proceedings of the Cambridge Philosophical Society*, vol. 43, no. 1, p. 50–67, 1947.

[23] W. F. Ames, *Numerical Methods for Partial Differential Equations*, 3rd ed. San Diego: Academic Press Inc, 1992.

[24] J. W. Ekin, *Experimental Techniques for Low-Temperature Measurements*. New York: Oxford University Press, 2007.

[25] J. R. Clem, "Two-dimensional vortices in a stack of thin superconducting films: A model for high-temperature superconducting multilayers," *Physical Review B*, vol. 43, no. 10, p. 7837–7846, 1991.

[26] W. B. Richardson, A. L. Pardhanani, G. F. Carey, and A. Ardelea, "Numerical effects in the simulation of Ginzburg–Landau models for superconductivity," *International Journal for Numerical Methods in Engineering*, vol. 59, no. 9, pp. 1251–1272, 2004.

[27] H. J. Fink, "Supercurrents through superconducting-normal-superconducting proximity layers. I. Analytic solution," *Phys. Rev. B*, vol. 14, no. 3, pp. 1028–1038, Aug. 1976.